SCIENCE CHINA Materials ARTICLES

mater.scichina.com link.springer.com

Published online 28 May 2021 | https://doi.org/10.1007/s40843-021-1652-2
Sci China Mater 2021, 64(10): 2601–2612

A new class of nitrobenzoic acid-based AIE photosensitizers for highly efficient photodynamic antibacterial therapy

Huanhuan Wang[1,2], Xiaohong Pan[1*], Yaqi Wang[1], Wenzhen Liu[1], Tao Dai[1,2], Binbin Yuan[1], Xueyuan Chen[1,2] and Zhuo Chen[1,2*]

ABSTRACT **Photodynamic therapy (PDT) has been drawing more and more attention in the antibacterial field. Traditional photosensitizers (PSs) tend to aggregate in aqueous media, which reduces the generation of reactive oxygen species (ROS) and seriously affects the photodynamic efficacy. Many efforts have been made to prevent aggregation of traditional PSs. By contrast, aggregation-induced emission PSs (AIE-PSs) take advantage of aggregation to boost ROS generation and fluorescence intensity. However, the efficacies of the reported antibacterial AIE-PSs are poor. Herein, we report a new class of highly effective antibacterial AIE-PSs based on nitrobenzoic acid structure. TTVBA, a negatively charged AIE-PS, can not only selectively kill spherical bacteria (*Staphylococcus aureus* (*S. aureus*)) rather than rod-shaped bacteria (*Escherichia coli* (*E. coli*)), but also be easily extended to several AIE-PSs (TTVBP1–3) with positive charges and broad-spectrum antibacterial activity. We demonstrate that TTVBP2 can kill 3.0 $\log_{10}$ of *S. aureus* at very low concentration (125 nmol L^{-1}), TTVBP3 can kill 4.7 $\log_{10}$ of *Staphylococcus epidermidis* (*S. epidermidis*) at a concentration of 1 μmol L^{-1} and 3.8 $\log_{10}$ of *E. coli* at 5 μmol L^{-1}, thus enabling them among the most effective antibacterial AIE-PSs reported so far. Meanwhile, these AIE-PSs exhibit excellent wash-free imaging ability for bacteria by simple mixing with bacteria. We thus envision that TTVBA, a nitrobenzoic acid-based extendable AIE-PS, provides a new route for the design of AIE-PSs in antibacterial treatment.**

Keywords: photodynamic antibacterial therapy, photosensitizer, aggregation-induced emission, reactive oxygen species, imaging

INTRODUCTION

With the long-term overuse and abuse of antibiotics, the number of drug-resistant bacteria is increasing, and thus bacterial infection has been a serious threat to human health [1,2]. Photodynamic therapy (PDT), which utilizes photosensitizers (PSs), light and oxygen to generate toxic reactive oxygen species (ROS) to destroy the external and internal structures of bacteria, is considered not susceptible to drug resistance and to be an effective way to solve this serious medical problem [3–8].

Traditional PSs, such as porphyrin, phthalocyanine and boron-dipyrromethene, are prone to forming aggregates in aqueous media [4,9]. The strong π-π stacking in the aggregate quenches the fluorescence, decreases the ROS generation, reduces the signal-to-noise ratio of bacterial imaging, and decreases the sterilization effect [10–14]. By contrast, aggregation-induced emission PSs (AIE-PSs) emit weak light in molecular species, but shine up upon aggregation due to the restriction of intramolecular motions which suppresses nonradiative decay and results in high ROS generation [11,12,15–17]. Since the first discovery of AIE phenomenon in 2001 [18], AIE-PSs have been successfully applied in the cell [12,19–26] and bacteria imaging and ablation [4,27–38]. In addition to the membrane-anchoring AIE-PS reported in 2019 that killed 99.9% (3.0 $\log_{10}$) of *Staphylococcus aureus* (*S. aureus*) at a concentration of 2 μmol L^{-1} and 99.9% of *E. coli* at 5 μmol L^{-1} [39], most reported antibacterial rates of AIE-PSs did not exceed 99% (2.0 $\log_{10}$). Therefore, more effective antibacterial AIE-PSs, especially AIE-PS backbones that can be easily added with different anchoring

[1] State Key Laboratory of Structural Chemistry, CAS Key Laboratory of Design and Assembly of Functional Nanostructures, Fujian Institute of Research on the Structure of Matter, Chinese Academy of Sciences, Fuzhou 350002, China
[2] University of Chinese Academy of Sciences, Beijing 100049, China
* Corresponding authors (emails: panxiaohong@fjirsm.ac.cn (Pan X); zchen@fjirsm.ac.cn (Chen Z))

groups for bacteria are still much needed.

In addition, due to the negative charges on the surface of bacteria, most PSs are designed to have positive charges, which bind to all bacteria through electrostatic interaction without selectivity [4,40,41]. To reduce the impact of off-target on microbial community (e.g., intestinal microflora), more and more attention has been paid to selective killing methods of harmful pathogens [42–45]. Recently, it has been reported that negatively charged nanospheres, driven by entropy gain, could adsorb selectively onto spherical bacteria, but not onto rod-shaped bacteria [3]. Verteporfin and chlorin e6 as the traditional PSs were preloaded into nano-micelles to prevent aggregation and quenching of ROS generation. The resulting photodynamic nanospheres with negative charges killed more than 99% of spherical bacteria but less than 1% of rod-shaped bacteria [3]. Rather than quenching ROS generation for traditional PSs [46], aggregation boosts ROS generation for AIE-PSs [47]. Therefore, AIE-PSs are promising candidates to form photodynamic nanospheres by simple aggregation without further decoration. Although some AIE luminogens with negative charges have been reported [48–50], few AIE-PSs with negative charges have been studied.

In this contribution, we designed and synthesized **TTVBA**, a novel extendable AIE-PS (Scheme 1). The nitrobenzoic acid fragment endows **TTVBA** with a negative charge in physiological environment. **TTVBA** as the backbone was extended to **TTVBP** and **TTVBP1–3** by coupling with piperazine and alkyl halides. **TTVBP1** has a positive charge near the backbone, while **TTVBP2** has a positive charge at the end of the chain (away from the backbone). **TTVBP3** is a hybrid of **TTVBP1** and **TTVBP2** with two positive charges. Their structure-function relationships toward narrow- and broad-spectrum bacterial ablation and imaging were evaluated. This study demonstrates that **TTVBA** is a promising AIE-PS backbone, which can be extended into AIE-PSs with high antibacterial efficiency.

EXPERIMENTAL SECTION

Chemicals

Singlet oxygen sensor green (SOSG) were obtained from Shanghai Aladdin Bio-Chem Technology Co., Ltd. Phosphate buffer saline (PBS, pH 7.4) used throughout the work was purchased from Dalian Meilun Biotechnology Co., Ltd. Silica gel, alumina and basic alumina were purchased from Shanghai Aladdin Bio-Chem Technology Co., Ltd. All solvents and materials were used as received without further purification. **TTVBA**, **TTVBP** and **TTVBP1–3** were pre-dissolved in dimethyl sulfoxide (DMSO, 1 mmol L^{-1}) throughout the experiments.

Instruments

^{1}H and ^{13}C NMR spectra were obtained on a Bruker BioSpin AVANCE III 400 MHz spectrometer or a JEOL EZC400S 400MHz spectrometer. High-resolution mass spectra (HRMS) were recorded on a Bruker Impact II Mass Spectrometer. Absorption and fluorescence spectra were measured on a BioTek Synergy™ 4 Multi-Mode Microplate Reader. The binding kinetics of AIE-PSs with bacteria and the uptake of AIE-PSs by bacteria were detected on a CytoFLEX flow cytometer (Beckman Coulter Inc., CA, USA). The images of bacteria were observed by an Olympus FluoView™ FV1000 confocal laser scanning microscope (CLSM). The particle sizes and zeta potentials were measured by a dynamic light scattering (DLS) instrument (Zetasizer 3000, Malvern Instruments, Ltd.). The morphologies were characterized by using a field-emission scanning electron microscope (SEM, JEOL-JSM-6700F) at 10 kV.

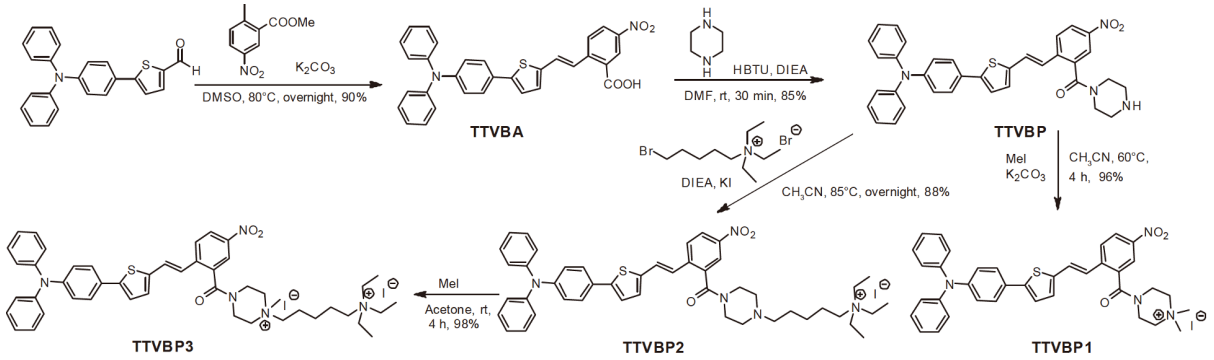

Scheme 1 Synthesis of **TTVBA** and its derivatives. HBTU: 2-(1*H*-benzotriazole-1-yl)-1,1,3,3-tetramethyluronium hexafluorophosphate; DIEA: *N*,*N*-diisopropylethylamine; DMF: *N*,*N*-dimethylformamide; MeI: iodomethane; rt: room temperature.

Bacterial strains and cultivation conditions

Gram-positive bacteria *S. aureus* (ATCC 6538), *Staphylococcus epidermidis* (*S. epidermidis*, ATCC 12228), *Enterococcus faecalis* (*E. faecalis*, ATCC 29212) and Gram-negative bacterium *Escherichia coli* (*E. coli*, ATCC 25922) were purchased from Beijing Zhongyuan Ltd. (China). They were grown in Luria-Bertani (LB) broth media (1% tryptone, 0.5% yeast extract, 1% NaCl, pH 7.0) at 37°C with shaking at 220 r min^{-1}. The number of bacteria was estimated by measuring the optical density at 600 nm to obtain 10^8 CFU mL^{-1} (colony forming unit, CFU).

Cell line and culture

The human normal liver cell line L-O2 was purchased from Shanghai Institute of Cell Biology, Chinese Academy of Sciences (China), and maintained in Dulbecco's Modified Eagle's Medium (DMEM) with 10% fetal bovine serum (Gibco, Invitrogen, Grand Island, NY, USA), 100 μg mL^{-1} penicillin and 100 μg mL^{-1} streptomycin (Gibco, Invitrogen, Grand Island, NY, USA) at 37°C with 5% CO_2.

Synthesis of TTVBA, TTVBP and TTVBP1–3

The synthetic methods and the characterizations of **TTVBA**, **TTVBP** and **TTVBP1–3** (^{1}H NMR, ^{13}C NMR and mass spectra) are detailed in the Supplementary information (Figs S1–S10).

Singlet oxygen generation

The generation of singlet oxygen in the photodynamic therapy of AIE-PSs under white-light irradiation was studied by using the molecular probe SOSG. In the presence of singlet oxygen, SOSG can react with singlet oxygen to produce SOSG endoperoxides (SOSG-EPs) that emit strong green fluorescence (λ_{ex} = 488 nm, λ_{em} = 520 nm). Typically, PBS (200 μL) containing SOSG (100 μmol L^{-1}) and AIE-PS (10 μmol L^{-1}) was irradiated for 20 min, and then the fluorescence intensity at 520 nm was recorded every 2 min. The solution with only SOSG was used as a control group.

Photodynamic antibacterial activity

The antibacterial activities of AIE-PSs were evaluated by the method of colony counting on an agar plate. The bacteria in PBS (10^7 CFU mL^{-1}, 1 mL) mixed with AIE-PSs were incubated in multiple-well plates for 5 min in the dark at 37°C. After 40 min of white-light irradiation (400–800 nm, 20 mW cm^{-2}), aliquots (100 μL) from each well were taken and serially diluted 10-fold in PBS. One hundred microlitre of each dilution was then dispersed on the LB solid agar plate to determine the CFU. One group without receiving light served as the control. The colonies were counted after incubation at 37°C for 16–24 h. Each experiment was performed independently at least three times.

Binding kinetics of AIE-PSs with bacteria

The binding kinetics of AIE-PSs with bacteria was monitored *via* a CytoFLEX flow cytometer at a fluorescent channel (PC5.5-A, λ_{ex} = 488 nm, λ_{em} = 665–715 nm). The cultured bacteria (OD_{600} = 0.6) were centrifuged and re-suspended in PBS (900 μL) by 10-fold dilution. After being mixed with PBS solution of AIE-PS (100 μmol L^{-1}, 100 μL), the fluorescence intensity was monitored for continuous 7 min. One group without adding AIE PS served as a control.

Uptake of AIE-PSs by bacteria

The uptake of AIE-PSs by bacteria was investigated *via* a CytoFLEX flow cytometer at a fluorescent channel (PC5.5-A, λ_{ex} = 488 nm, λ_{em} = 665–715 nm). In brief, bacteria (OD_{600} = 0.6) were first incubated with AIE-PS (10 μmol L^{-1}) in PBS at 37°C for 5 min in the dark. After centrifugation at 5000 r min^{-1} for 3 min, the precipitate was resuspended in PBS by 10-fold dilution. The fluorescence intensity was measured and analyzed on a CytoFLEX flow cytometer. One group without adding AIE PSs served as a control. Each experiment was performed independently at least three times.

Zeta potential (ζ) measurements

The zeta potential measurements were conducted for bacteria incubated with AIE-PSs using the same device for DLS measurements. In brief, bacteria (OD_{600} = 0.6) were incubated with AIE-PS (10 μmol L^{-1}) in PBS for 5 min in the dark at 37°C. Following that, the bacteria were harvested after centrifugation at 5000 r min^{-1} for 3 min and being washed twice with water. The bacteria were then resuspended in water by 10-fold dilution for zeta potential measurements. The bacterial samples that were not incubated with AIE-PS were used as negative controls.

Bacterial imaging

Bacteria (OD_{600} = 0.6) were harvested by centrifugation at 5000 r min^{-1} for 3 min and resuspended in PBS (990 μL) to receive a concentration of 10^9 CFU mL^{-1}. After being mixed with AIE-PS (1 mmol L^{-1} in DMSO, 10 μL) and incubated for 20 min in the dark at 37°C, the bacteria were re-dispersed at room temperature. The suspension

(15 μL) was then transferred onto a glass slide and covered with a glass coverslip (18 mm × 18 mm). Images were taken on an Olympus FluoView™ FV1000 CLSM (λ_{ex} = 488 nm, λ_{em} = 570–1000 nm).

Photostability test of AIE-PSs

The photostability of AIE-PSs was evaluated by measuring the fluorescence intensities of AIE-PSs on *S. aureus* by continuous irradiation (λ_{ex} = 488 nm) and sequential scanning (every 5 s, 120 times) on an Olympus FluoView™ FV1000 CLSM.

Biocompatibility tests of AIE-PSs

The biocompatibility of AIE-PSs was evaluated by measuring the phototoxicity and dark toxicity of AIE-PSs to L-O2 cells using MTT (3-(4,5-dimethylthiazol-2-yl)-2,5-diphenyltetrazolium bromide) assay. In brief, aliquots (100 μL) of L-O2 cells (10^4 cells) were cultured at 37°C in a 96-well plate, allowed to attach overnight, and then left untreated or treated with growth medium containing AIE-PSs with different concentrations (6.25, 12.5, 25, 50, 100 μmol L^{-1}) for 2 h. The cultures were illuminated with white light (20 mW cm^{-2}) for 40 min, followed by incubation for 24 h. Freshly prepared MTT solution (5 mg mL^{-1}, 10 μL) was then added into each well, followed by incubation for another 4 h. After removing the MTT containing medium, 150 μL of DMSO was added to dissolve the Formosan crystals. The optical density of solution was measured by enzyme-linked immunosorbent assay (ELISA) at 490 nm. The value of cell viability was determined according to the following formula: cell viability (%) = (mean absorbance of the treatment group/mean absorbance of the control group) × 100%. The dark toxicity of AIE-PSs to L-O2 cells in the absence of light was measured in parallel.

Statistical analysis

All data represent group means and standard errors (SEs) of the mean. The data of antibacterial activity were analyzed by two-way analyses of variance (ANOVA). The data of binding capacity of AIE-PSs by bacteria was analyzed by one-way ANOVA. Individual group means were compared by the Newman-Keuls multiple range test.

RESULTS AND DISCUSSION

Molecular design and synthesis

As shown in Scheme 1, Knoevenagel condensation of triphenylamine-thiophene and methyl 2-methyl-5-nitrobenzoate afforded **TTVBA** as a red precipitate in 90% yield without further purification. The following amidation of **TTVBA** with piperazine gave **TTVBP** in a yield of 85%. Alkylation of **TTVBP** with methyl iodide and 5-bromo-*N*,*N*,*N*-triethylpentan-1-aminium bromide provided **TTVBP1**, **TTVBP2** and **TTVBP3**, respectively in high yield. **TTVBA** as the backbone structure consists of a triphenylamine moiety (electron donor and spacer to prevent π-π stacking in the aggregate), a thiophene fragment (electron donor and π-bridge), a carbon-carbon double bond (π-bridge) and a nitrobenzoic acid unit (electron acceptor). This structure possesses extended π-conjugation and strong donor-acceptor effect which will cause the separation of the highest occupied molecular orbital (HOMO) and the lowest unoccupied molecular orbital (LUMO), decrease the singlet-triplet energy gap and thus increase the ROS generation capacity [23,45,51]. The carboxylic acid moiety, working as an electron withdrawing group, will not only bring **TTVBA** a negative charge in physiological environment, but also make **TTVBA** a versatile backbone to conjugate with amines, alcohols, amino acids, peptides and proteins to achieve different functionalities.

Physical properties

Considering **TTVBP** is also the backbone of **TTVBP1–3**, we chose **TTVBA** and **TTVBP** as the representatives of new AIE-PSs to study their physical properties. As depicted in Fig. 1a, the absorptions of **TTVBA** and **TTVBP** in DMSO are broad from 400 to 550 nm in the visible-light range, and the peaks locate at 447 and 457 nm, respectively. The AIE features of **TTVBA** and **TTVBP** were demonstrated by testing their emission in a mixed solvent (DMSO/toluene) with different toluene fractions (Fig. 1b–d). **TTVBA** and **TTVBP** behaved similarly in these tests. No emission was observed in DMSO (well dissolved), but the emission enhanced gradually with the increase of toluene fraction up to 90%. A dramatic enhancement of emission was observed when the toluene fraction was increased to 95% and 99%, and their maximum peaks (around 640 nm) were 360 times higher than those in pure DMSO solution. This emission enhancement is mostly due to the restriction of intramolecular motions when AIE-PSs aggregate in toluene (poor solvent). Because of the donor-acceptor structure in **TTVBA** and **TTVBP**, the emission peaks blue-shift gradually from DMSO (polar solvent) to toluene (nonpolar solvent), which is a typical twisted intramolecular charge transfer effect [52,53]. The emission and absorption characteristics of **TTVBP1–3** (Fig. S11) were similar to that of

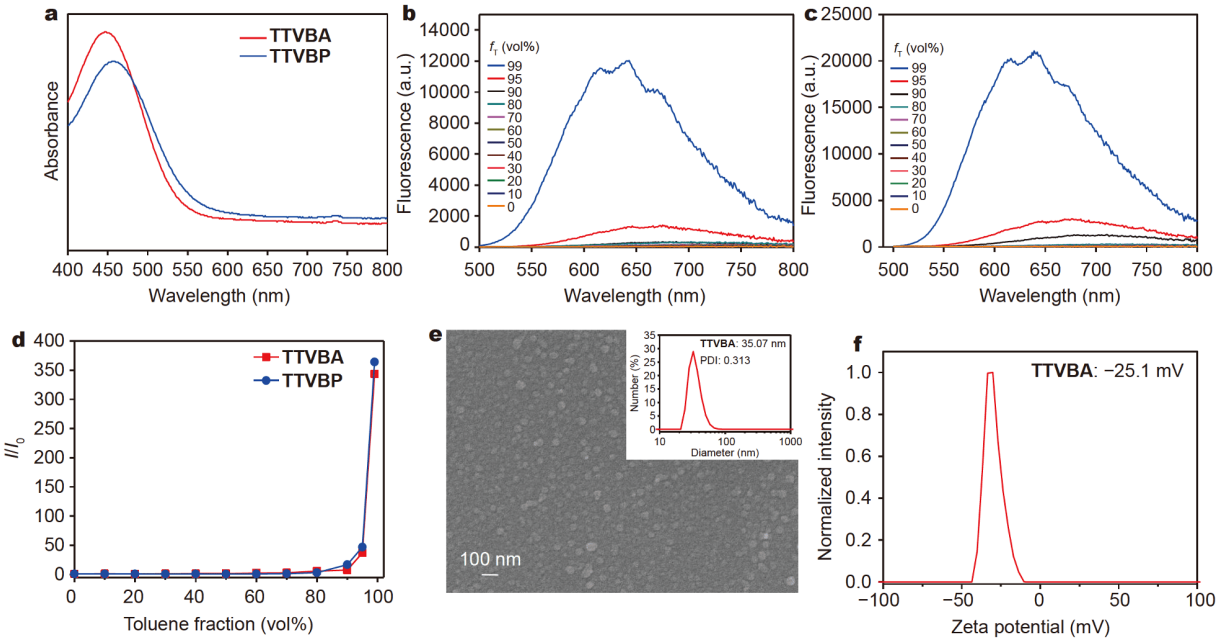

Figure 1 Physical properties of AIE-PSs **TTVBA** and **TTVBP**. (a) Absorption spectra of **TTVBA** and **TTVBP** in DMSO. Photoluminescence spectra of (b) **TTVBA** (10^{-5} mol L^{-1}) and (c) **TTVBP** (10^{-5} mol L^{-1}) in mixed solvents with different toluene fractions (DMSO/toluene). (d) Plots of relative emission intensity of **TTVBA** and **TTVBP** *versus* toluene fraction. I_0 and I are the peak values of photoluminescence intensities in DMSO and in mixed solvent (DMSO/toluene), respectively. (e) SEM image of **TTVBA** (10^{-6} mol L^{-1}) in 1% DMSO/water and hydrodynamic size distribution of **TTVBA** (10^{-6} mol L^{-1}) in 1% DMSO/PBS (inset). (f) Zeta potential of **TTVBA** (10^{-6} mol L^{-1}) in 1% DMSO/water.

TTVBP. The different intensities among them may be due to the difference of charge number and position, leading to their different solubilities and aggregation intensities in the solvent. DLS analysis (Fig. 1e inset and 1f) demonstrated that **TTVBA** formed negatively charged nanospheres in physiological environment (~35 nm diameter, −25 mV zeta potentials). The image obtained from SEM (Fig. 1e) showed that the nanospheres have an average diameter of ~39 nm.

Theoretical calculation and singlet oxygen generation ability

In order to further evaluate the structural design of our AIE-PSs, density functional theory (DFT) calculations of **TTVBA** and **TTVBP** were performed (Fig. 2a and b). The calculated HOMO-LUMO energy gaps of **TTVBA** and **TTVBP** are 2.37 and 2.49 eV, respectively. Their LUMOs are mainly delocalized at nitrobenzene and carbon-carbon double bond units, while triphenylamine and thiophen groups dominate the HOMOs. The strong donor-acceptor effect separates their HOMO and LUMO. Because of this separation, we were expecting their high ROS generation ability [54].

Among ROS, including superoxide and hydroxyl radicals, singlet oxygen is the primary cytotoxic agent to destruct biological tissues and cells in PDT because of its strong diffusibility and high oxidative efficiency [55–57]. Therefore, the singlet oxygen generation abilities of **TTVBA** and **TTVBP** were evaluated in this study using SOSG, a specific singlet oxygen probe. Commercial PSs Rose Bengal (RB) and chlorin e6 (Ce6) were used as references in current study. SOSG alone was non-fluorescent, while its fluorescence gradually enhanced when exposed to white light in the presence of above PSs, indicating the generation of singlet oxygen (Fig. 2c). The fluorescence intensity of SOSG treated with **TTVBA** or **TTVBP** was significantly higher than that of SOSG treated with RB or Ce6. Furthermore, the fluorescence intensity of SOSG treated with **TTVBA** was stronger than that of SOSG treated with **TTVBP**, demonstrating that **TTVBA** has stronger singlet oxygen generation ability than **TTVBP**.

Photodynamic antibacterial study

As both **TTVBA** and **TTVBP** have strong singlet oxygen generation abilities, it motivated us to explore the photodynamic antibacterial performances of **TTVBA** and **TTVBP1–3** against Gram-positive spherical *S. aureus* and Gram-negative rod-shaped *E. coli* under white-light irradiation (400–800 nm, 20 mW cm^{-2}) for 40 min. The

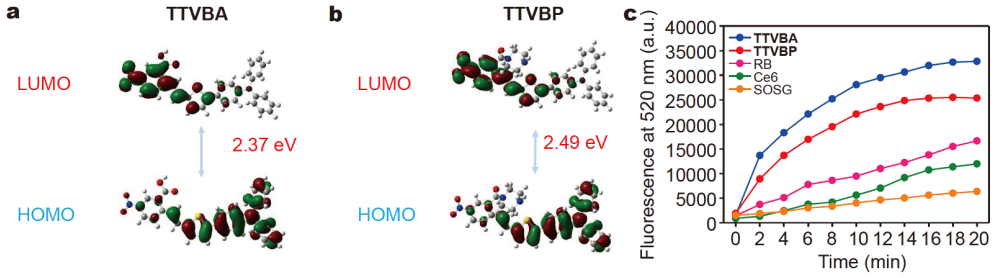

Figure 2 Theoretical calculation and singlet oxygen generation abilities of AIE PSs **TTVBA** and **TTVBP**. Theoretical calculations for frontier molecular orbitals of (a) **TTVBA** and (b) **TTVBP** were performed by using the density functional theory (DFT) at B3LYP/6-31G* level *via* the Gaussian 09 program. (c) Singlet oxygen produced by **TTVBA** and **TTVBP**.

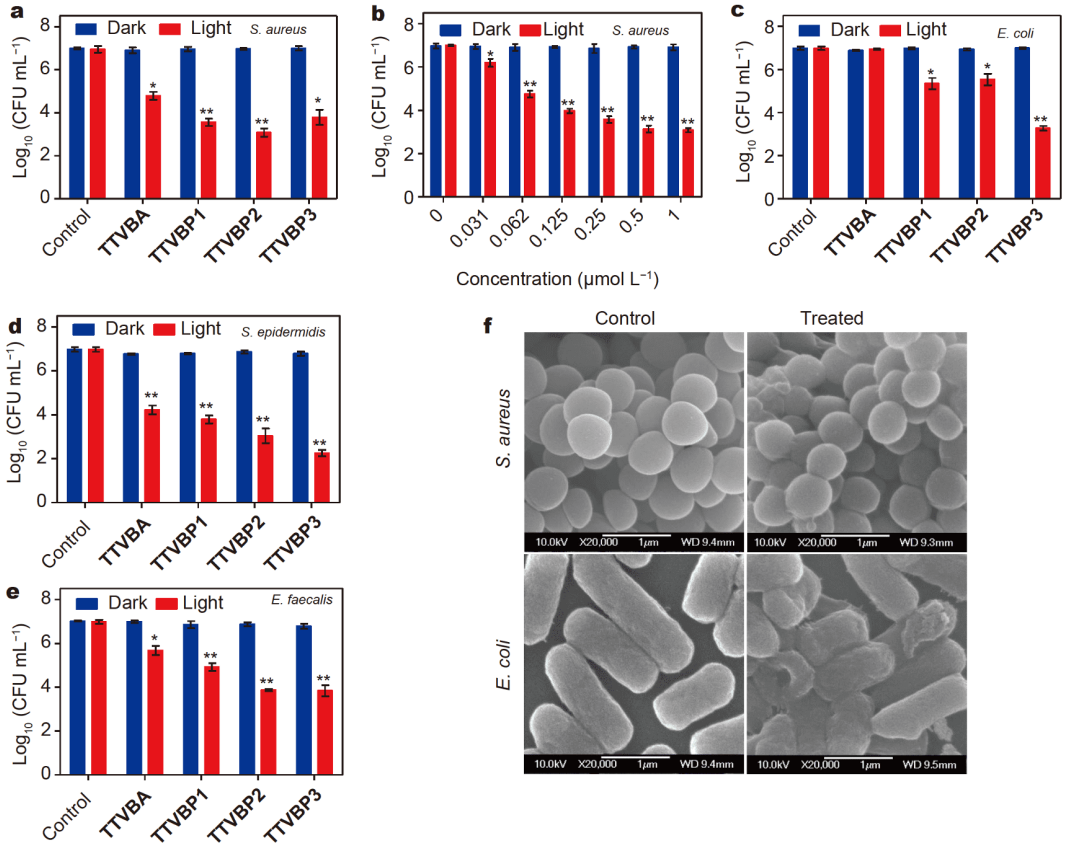

Figure 3 Photodynamic antibacterial activities of AIE-PSs. (a) Photodynamic antibacterial activities of AIE-PSs (10^{-6} mol L^{-1}) against *S. aureus* under white-light irradiation (20 mW cm^{-2}, 40 min). (b) Dose-response relationship of **TTVBP2** against *S. aureus* under white-light irradiation. Photodynamic antibacterial activities of AIE-PSs against (c) *E. coli* (5×10^{-6} mol L^{-1}), (d) *S. epidermidis* (10^{-6} mol L^{-1}) and (e) *E. faecalis* (10^{-6} mol L^{-1}) under white-light irradiation. (f) SEM images of *S. aureus* and *E. coli* before and after treatment with **TTVBP2** under white-light irradiation. Data are given as mean ± SE (n = 3). * and ** indicate significant differences ($P < 0.05$ and $P < 0.01$, respectively) from the corresponding control group.

antibacterial effect was demonstrated by traditional agar plate CFU counting method. **TTVBP** was not further investigated because it exists as a neutral molecule and can neither kill nor stain *S. aureus* or *E. coli* in the pre-experiments. As shown in Fig. 3a, **TTVBP1–3** (1 μmol L^{-1}) had significant scavenging effects on *S. aureus* (3.3–4.0 $\log_{10}$) compared with **TTVBA** (2.2 $\log_{10}$ = 99.2%). This may be due to the fact that negatively charged **TTVBA** nanospheres cannot bind to bacteria as strong as positively charged **TTVBP1–3** which interact with bacteria by electrostatic adsorption. No dark toxicity to *S. aureus* was found in this study. Taking **TTVBP2** as

an example, the dose-response relationship of **TTVBP2** against *S. aureus* was explored (Fig. 3b). **TTVBP2** had a dose-dependent bactericidal activity against *S. aureus*, killing 3.0 $\log_{10}$ (99.9%) of *S. aureus* at a concentration of 125 nmol L^{-1}. To the best of our knowledge, this is the first report describing that AIE-PS has good bactericidal activity at such a low concentration (125 nmol L^{-1}).

The photodynamic antibacterial activities of AIE-PSs (5 μmol L^{-1}) against *E. coli* were illustrated in Fig. 3c. Among the AIE-PSs investigated, **TTVBP3** had the strongest bactericidal effect on *E. coli* with a killing rate of 3.8 $\log_{10}$ (the killing rate of **TTVBP1** and **TTVBP2** to *E. coli* was 1.7 $\log_{10}$ and 1.5 $\log_{10}$, respectively), making **TTVBP3** one of the most effective AIE-PSs reported so far to kill *E. coli*. No cytotoxicity of **TTVBA** was found to *E. coli*, mainly because the negatively charged **TTVBA** nanospheres cannot bind to rod-shaped bacteria [3]. Similarly, no dark toxicity to *E. coli* was observed in this study. In a word, **TTVBP1–3** are excellent broad-spectrum antibacterial AIE-PSs, while **TTVBA** is a potential narrow-spectrum antibacterial AIE-PS that can kill spherical bacteria instead of rod-shaped bacteria.

We further investigated the antibacterial effects of AIE-PSs against *S. epidermidis* and *E. faecalis*. As shown in Fig. 3d and e, AIE-PSs (1 μmol L^{-1}) were efficient to kill *S. epidermidis* (3.1–4.7 $\log_{10}$) in the presence of white-light irradiation (40 min, 20 mW cm^{-2}). By comparison, *E. faecalis* was more tolerant to PDT treatment due to its thick cell wall. The killing rates of **TTVBA** and **TTVBP1** (1 μmol L^{-1}) were 1.3 $\log_{10}$ and 2.1 $\log_{10}$, respectively. It is worth mentioning that **TTVBP2** and **TTVBP3** could kill 3.2 $\log_{10}$ of *E. faecalis*.

In order to gain more information about the underlying mechanisms, micrographs of *S. aureus* or *E. coli* treated with **TTVBP2** under white-light irradiation (40 min, 20 mW cm^{-2}) were obtained by SEM (Fig. 3f). It was observed that the outer surfaces of both *S. aureus* and *E. coli* became rough, dented and damaged (fusion of cell walls and leakage of intracellular contents) after the PDT with **TTVBP2**.

Binding capacity and bacterial imaging

TTVBA is the backbone of **TTVBP1–3**, and they differ in the functional groups (alkylated piperazine with positive charges) that help them bind to bacteria. Therefore, their different antibacterial efficiencies are mostly due to their different binding capacities with bacteria [4]. When AIE-PSs aggregate or bind to cell membrane, their intramolecular motion is restricted, which suppresses the nonradiative decay and results in ROS generation and light emission [45]. Accordingly, the fluorescence intensity of AIE-PSs on bacteria reflects their binding capacities with bacteria [4]. This makes it possible to detect the binding kinetics between AIE-PSs and bacteria by tracking the fluorescence change on bacteria using a flow cytometer (Fig. 4, Figs S12–S14) [41]. The fluorescence intensity of *S. aureus* reached a maximum value (29-fold increased) within 3-min incubation with AIE-PSs, while that of *E. coli* hardly changed when treated with **TTVBA**, indicating that **TTVBA** was bound to *S. aureus*, but not to *E. coli*. This phenomenon is consistent with the selective killing effect of **TTVBA** we observed previously on *S. aureus* rather than *E. coli*. On the contrary, *E. coli* incubated with **TTVBP1–3** exhibited strong fluorescence intensity in 3 min, demonstrating the binding activity of **TTVBP1–3** with *E. coli*. It was noticeable that the fluorescence intensity of **TTVBP3** was 1.5-fold higher than those of **TTVBP1** and **TTVBP2**, revealing the strongest binding capacity of **TTVBP3** with *E. coli*. These results may be due to the fact that **TTVBP3** has two positive charges, which could replace the divalent cations (Ca^{2+} or Mg^{2+}) on lipid A that stabilize the lipopolysaccharide (LPS) structure, and interact strongly with the negatively charged LPS on the outer membrane of Gram-negative bacteria. The resulting unstable LPS coating forms "cracks" in the permeability barrier, which enable **TTVBP3** to penetrate into the periplasmic space [58,59]. The different binding capacities of our AIE-PSs with bacteria suggested that alkylated piperazine with two positive charges could be an effective bacterial membrane-anchoring group.

To further investigate the binding site of bacteria and AIE-PSs, zeta potential of bacteria, which reflects the surface charge of bacteria, was measured in this study. The positive charges of **TTVBP1–3** could be exposed on the surface of bacteria if they only bound to the surface of bacteria, making the zeta potential of bacteria more positive [60,61]. However, no change in zeta potential of *S. aureus* or *E. coli* was observed when treated with **TTVBP1–3** (Fig. S15), indicating that **TTVBP1–3** can effectively insert into the bacterial cell wall instead of just binding to the bacterial surface [45].

TTVBA, a negatively charged nanosphere, was found to bind onto spherical-like *S. aureus* rather than rod-shaped *E. coli*, thus keeping zeta potential of *E. coli* unchanged. On the other hand, **TTVBA** lighted up *S. aureus* as strongly as **TTVBP1–3** did in 1% DMSO/PBS (Fig. 4b), but the fluorescence of **TTVBA** nanospheres was vanishingly weak in this solvent compared with that in 1% DMSO/toluene (Fig. S16). Therefore, we hypothesized

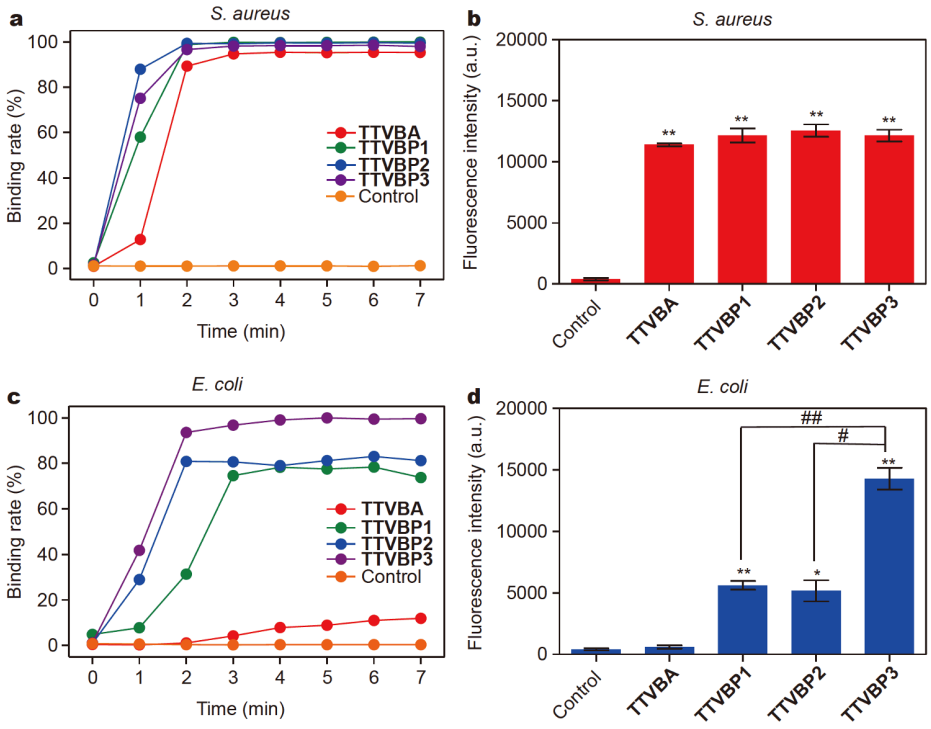

Figure 4 Binding kinetics between AIE-PSs and (a) *S. aureus* or (c) *E. coli*, and the fluorescence intensities of (b) *S. aureus* and (d) *E. coli* after 5-min incubation with AIE-PSs (10^{-5} mol L^{-1}). Data are given as mean ± SE (n = 3). * and ** indicate significant differences ($P < 0.05$ and $P < 0.01$, respectively) from the corresponding control group. # and ## indicate significant differences ($P < 0.05$ and $P < 0.01$, respectively) between two groups.

that **TTVBA** nanospheres did not accumulate on the surface of *S. aureus*. Furthermore, the intramolecular motions of AIE-PSs, which will consume the excited state energy, cannot be restricted on the bacterial membrane surface, and thus no fluorescence signal can be detected on the bacterial surface if AIE-PSs only bind to the bacterial surface [45]. Taken together, we assumed that **TTVBA** nanospheres were decomposed on the hydrophobic surface of *S. aureus*, and the resulting **TTVBA** molecules intercalated into the porous cell wall, keeping the zeta potential of *S. aureus* unchanged.

In virtue of strong fluorescence of our AIE-PSs on bacteria detected by flow cytometer, the fluorescence imaging of bacteria was viewed under a CLSM after mixing bacteria with AIE-PSs without washing. As shown in Fig. 5a, when *S. aureus* were mixed with **TTVBA**, the fluorescence of *S. aureus* can be clearly visualized, while that of *E. coli* cannot be seen when *E. coli* were mixed with **TTVBA** or **TTVBA** plus *S. aureus*, demonstrating that **TTVBA** is more selective for *S. aureus* than for *E. coli*. The luminescent intensities of *S. aureus* treated with **TTVBP1–3** were similar (Fig. 5b), while the luminescent intensity of *E. coli* treated with **TTVBP3** was significantly enhanced compared with that of **TTVBP1** or **TTVBP2** (Fig. 5c). These phenomena are consistent with the high efficiency of **TTVBP1–3** against *S. aureus* and the best killing effect of **TTVBP3** on *E. coli*, demonstrating that the binding ability of AIE-PSs to bacteria affects its fluorescence intensity and photodynamic antibacterial ability. Importantly, all samples were prepared by simple mixing, whereas all images had outstanding image contrast to the background, demonstrating the excellent wash-free imaging ability of **TTVBA** and **TTVBP1–3** toward bacteria.

Stability of AIE-PSs

The photostability of AIE-PS on *S. aureus* was tested by continuous irradiation (λ_{ex} = 488 nm) and sequential scanning with CLSM every 5 s for 120 times. As shown in Fig. 6a, **TTVBP1–3** have higher photobleaching resistances than **TTVBA**, which is probably due to the reactive carboxylic acid group toward the adjacent vinyl group in **TTVBA**, or the instability of **TTVBA** nanospheres under illumination. The relatively weak photostability of **TTVBA** explained why the fluorescence intensity of **TTVBA** on *S. aureus* was similar to

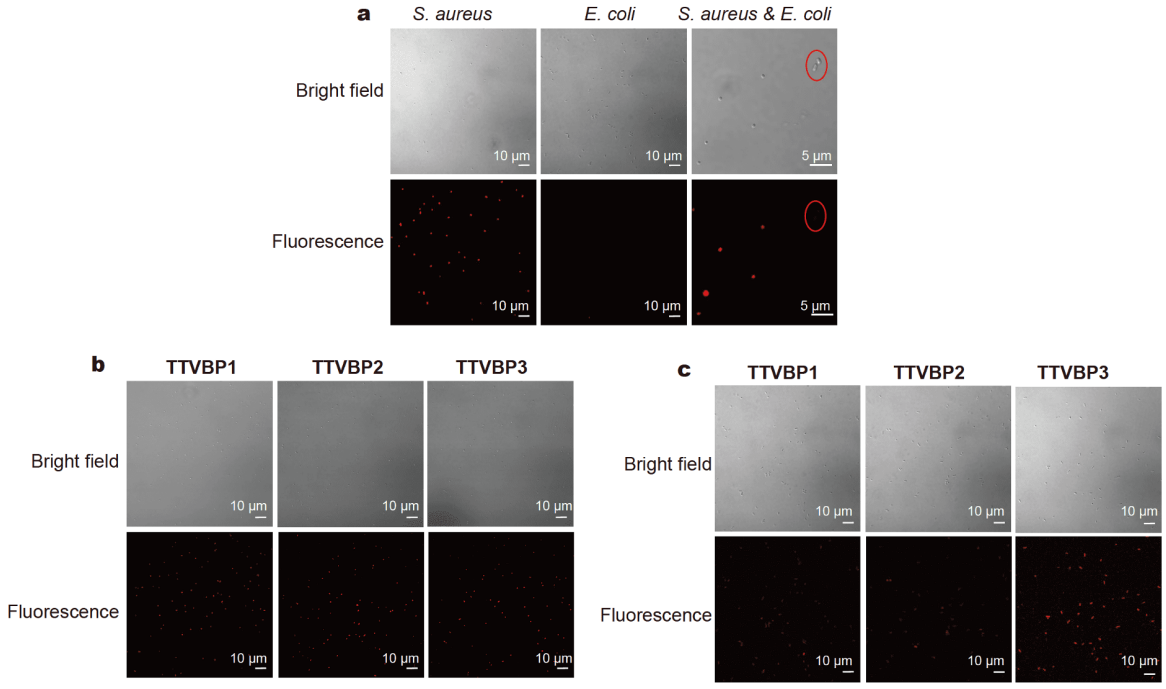

Figure 5 Bacterial imaging after mixing with AIE-PSs. (a) Selective bacterial imaging capability of **TTVBA** under a CLSM. (b) *S. aureus* and (c) *E. coli* imaging after mixing with AIE-PSs without washing.

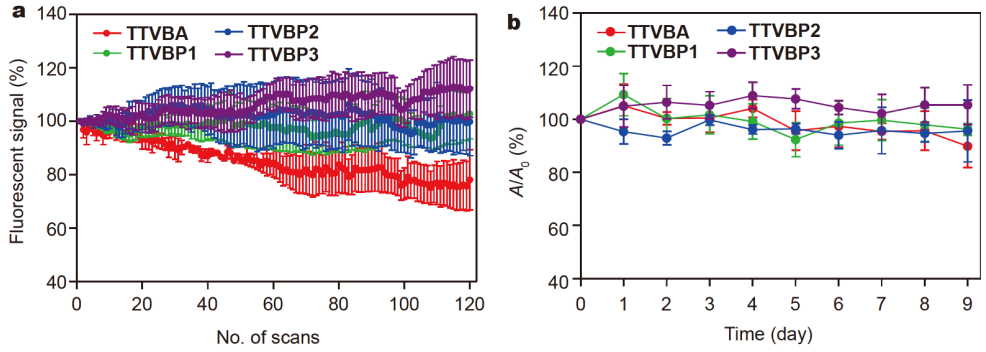

Figure 6 Stability of AIE-PSs investigated (10 μmol L^{-1}). (a) Photostability of AIE-PSs on *S. aureus*. (b) Dark stability of AIE-PSs in PBS. A_0 and A are the absorption peak values at 450 nm in PBS on and after the first day, respectively. Data are given as mean ± SE (n = 3).

TTVBP1–3, but its bactericidal effect on *S. aureus* was inferior to **TTVBP1–3**.

Meanwhile, the dark stability of AIE-PSs in PBS was measured by tracking their daily light absorptions for 9 consecutive days at room temperature. As shown in Fig. 6b, the intensity of the absorption peak (450 nm) remained unchanged, indicating that these AIE-PSs were stable in PBS.

Biocompatibility test

The biocompatibility of above AIE-PS was evaluated by acute toxicity test on human normal hepatocyte cell line (L-O2). In brief, different concentrations of AIE-PSs were incubated with L-O2 cells for 2 h, followed by irradiation with white light (20 mW cm^{-2}) for 40 min. As illustrated in Fig. 7, no cytotoxicity or dark toxicity was observed among AIE-PSs investigated at concentrations up to 12.5 μmol L^{-1}. **TTVBP2** showed slight cytotoxicity at a concentration of 12.5 μmol L^{-1} which is 100 times higher than its effective antibacterial dose (125 nmol L^{-1}). Therefore, these AIE-PSs have excellent biocompatibility.

CONCLUSION

TTVBA, a nitrobenzoic acid-based AIE-PS with high

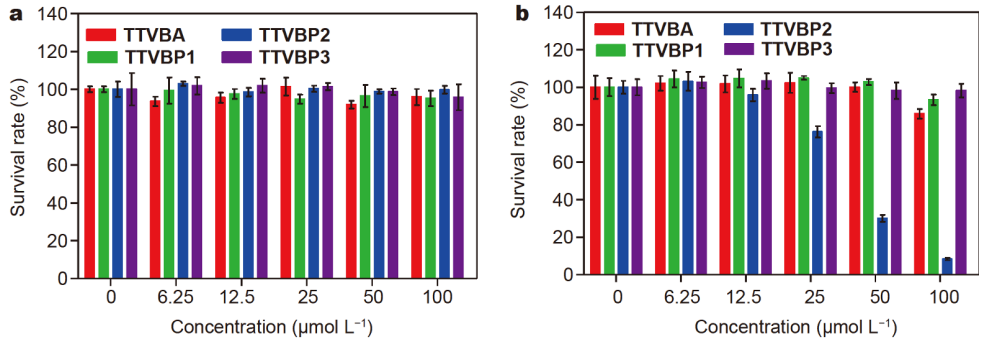

Figure 7 Biocompatibilities of AIE-PSs investigated. (a) Dark toxicity and (b) phototoxicity of AIE-PSs on human normal hepatocyte cell line (L-O2). Phototoxicity was performed under white-light irradiation (20 mW cm^{-2}, 40 min). Data are given as mean ± SE (n = 3).

ROS generation ability, was rationally designed and efficiently prepared without the need of further purification. The negatively charged **TTVBA** nanospheres selectively imaged and killed sphere-shaped *S. aureus*, showing their narrow-spectrum antibacterial ability. When coupled with piperazine, **TTVBA** was easily extended to **TTVBP**, which was then alkylated to give **TTVBP1–3** with positive charges. **TTVBP1–3** can efficiently image and kill both *S. aureus* and *E. coli*. In particular, **TTVBP2** killed 3.0 $\log_{10}$ of *S. aureus* at a very low concentration (125 nmol L^{-1}), **TTVBP3** killed 4.7 $\log_{10}$ of *S. epidermidis* at a concentration of 1 μmol L^{-1} and 3.8 $\log_{10}$ of *E. coli* at 5 μmol L^{-1}, which makes them among the most effective antibacterial AIE-PSs reported so far. Meanwhile, these AIE-PSs have good photostability and wash-free imaging ability for bacteria with strong contrast to the background. The antibacterial effects of these AIE-PSs were directly proportional to the fluorescence intensity of the bacteria bound with them, suggesting that the bacterial binding ability of AIE-PS determines its photodynamic antibacterial ability. These entire successful examples demonstrate that **TTVBA** is an extendable AIE-PS backbone with excellent photodynamic and imaging capabilities, and it can be easily extended to AIE-PSs with various functionalities in biomedical studies, including biological imaging, antibacterial and antitumor functions. Moreover, the strong binding of these AIE-PSs to bacteria indicates that alkylated piperazine with positive charges is an effective anchoring group for bacterial membrane, which successfully improves the antibacterial efficacy of AIE-PSs.

Received 1 January 2021; accepted 22 February 2021; published online 28 May 2021

1 Blair JMA, Webber MA, Baylay AJ, *et al.* Molecular mechanisms of antibiotic resistance. Nat Rev Microbiol, 2015, 13: 42–51
2 Moore CE. Changes in antibiotic resistance in animals. Science, 2019, 365: 1251–1252
3 Yang B, Gao F, Li Z, *et al.* Selective entropy gain-driven adsorption of nanospheres onto spherical bacteria endows photodynamic treatment with narrow-spectrum activity. J Phys Chem Lett, 2020, 11: 2788–2796
4 Shi X, Sung SHP, Chau JHC, *et al.* Killing G(+) or G(−) bacteria? The important role of molecular charge in AIE-active photosensitizers. Small Methods, 2020, 4: 2000046
5 Dai T, Ye F, Hu P, *et al.* A strategy for enhanced tumor targeting of photodynamic therapy based on *Escherichia coli*-driven drug delivery system. Sci China Mater, 2021, 64: 232–240
6 Jia HR, Zhu YX, Chen Z, *et al.* Cholesterol-assisted bacterial cell surface engineering for photodynamic inactivation of Gram-positive and Gram-negative bacteria. ACS Appl Mater Interfaces, 2017, 9: 15943–15951
7 Li J, Sun W, Yang Z, *et al.* Rational design of self-assembled cationic porphyrin-based nanoparticles for efficient photodynamic inactivation of bacteria. ACS Appl Mater Interfaces, 2020, 12: 54378–54386
8 Sun YD, Zhu YX, Zhang X, *et al.* Role of cholesterol conjugation in the antibacterial photodynamic therapy of branched polyethylenimine-containing nanoagents. Langmuir, 2019, 35: 14324–14331
9 Guan Q, Fu DD, Li YA, *et al.* Bodipy-decorated nanoscale covalent organic frameworks for photodynamic therapy. iScience, 2019, 14: 180–198
10 Hong Y, Lam JW, Tang BZ. Aggregation-induced emission. Chem Soc Rev, 2011, 40: 5361–538
11 Yang W, Ling B, Hu B, *et al.* Synergistic *N*-heterocyclic carbene/palladium-catalyzed umpolung 1,4-addition of aryl iodides to enals. Angew Chem Int Ed, 2020, 59: 161–166
12 Xu W, Lee MMS, Nie JJ, *et al.* Three-pronged attack by homologous far-red/NIR AIEgens to achieve 1+1+1>3 synergistic enhanced photodynamic therapy. Angew Chem Int Ed, 2020, 59: 9610–9616
13 Li X, Lee S, Yoon J. Supramolecular photosensitizers rejuvenate photodynamic therapy. Chem Soc Rev, 2018, 47: 1174–1188
14 Li S, Zou Q, Li Y, *et al.* Smart peptide-based supramolecular photodynamic metallo-nanodrugs designed by multicomponent coordination self-assembly. J Am Chem Soc, 2018, 140: 10794–10802
15 Mei J, Leung NLC, Kwok RTK, *et al.* Aggregation-induced emis-

sion: Together we shine, united we soar! Chem Rev, 2015, 115: 11718–11940
16 Jiang N, Shen T, Sun JZ, *et al.* Aggregation-induced emission: Right there shining. Sci China Mater, 2019, 62: 1227–1235
17 Zhao L, Liu Y, Xing R, *et al.* Supramolecular photothermal effects: A promising mechanism for efficient thermal conversion. Angew Chem Int Ed, 2019, 59: 3793–3801
18 Luo J, Xie Z, Lam JWY, *et al.* Aggregation-induced emission of 1-methyl-1,2,3,4,5-pentaphenylsilole. Chem Commun, 2001, 21: 1740–1741
19 Qi J, Duan X, Liu W, *et al.* Dragonfly-shaped near-infrared AIEgen with optimal fluorescence brightness for precise image-guided cancer surgery. Biomaterials, 2020, 248: 120036
20 Chong KC, Hu F, Liu B. AIEgen bioconjugates for specific detection of disease-related protein biomarkers. Mater Chem Front, 2019, 3: 12–24
21 Cai X, Liu B. Aggregation-induced emission: Recent advances in materials and biomedical applications. Angew Chem Int Ed, 2020, 59: 9868–9886
22 Liu Z, Zou H, Zhao Z, *et al.* Tuning organelle specificity and photodynamic therapy efficiency by molecular function design. ACS Nano, 2019, 13: 11283–11293
23 Wang D, Lee MMS, Shan G, *et al.* Highly efficient photosensitizers with far-red/near-infrared aggregation-induced emission for *in vitro* and *in vivo* cancer theranostics. Adv Mater, 2018, 30: 1802105
24 Han W, Zhang S, Deng R, *et al.* Self-assembled nanostructured photosensitizer with aggregation-induced emission for enhanced photodynamic anticancer therapy. Sci China Mater, 2019, 63: 136–146
25 Xu M, Wang X, Wang Q, *et al.* Analyte-responsive fluorescent probes with AIE characteristic based on the change of covalent bond. Sci China Mater, 2019, 62: 1236–1250
26 Liu S, Li Y, Kwok RTK, *et al.* Structural and process controls of AIEgens for NIR-II theranostics. Chem Sci, 2021, 12: 3427–3436
27 Chen J, Gao M, Wang L, *et al.* Aggregation-induced emission probe for study of the bactericidal mechanism of antimicrobial peptides. ACS Appl Mater Interfaces, 2018, 10: 11436–11442
28 Roy E, Nagar A, Chaudhary S, *et al.* AIEgen-based fluorescent nanomaterials for bacterial detection and its inhibition. ChemistrySelect, 2020, 5: 722–735
29 Zhao E, Chen Y, Chen S, *et al.* A luminogen with aggregation-induced emission characteristics for wash-free bacterial imaging, high-throughput antibiotics screening and bacterial susceptibility evaluation. Adv Mater, 2015, 27: 4931–4937
30 Zhao N, Li P, Zhuang J, *et al.* Aggregation-induced emission luminogens with the capability of wide color tuning, mitochondrial and bacterial imaging, and photodynamic anticancer and antibacterial therapy. ACS Appl Mater Interfaces, 2019, 11: 11227–11237
31 Zehra N, Dutta D, Malik AH, *et al.* Fluorescence resonance energy transfer-based wash-free bacterial imaging and antibacterial application using a cationic conjugated polyelectrolyte. ACS Appl Mater Interfaces, 2018, 10: 27603–27611
32 Zhu S, Wang X, Yang Y, *et al.* Conjugated polymer with aggregation-directed intramolecular Förster resonance energy transfer enabling efficient discrimination and killing of microbial pathogens. Chem Mater, 2018, 30: 3244–3253
33 Panigrahi A, Are VN, Jain S, *et al.* Cationic organic nanoaggregates as AIE luminogens for wash-free imaging of bacteria and broad-spectrum antimicrobial application. ACS Appl Mater Interfaces, 2020, 12: 5389–5402
34 Lee MMS, Xu W, Zheng L, *et al.* Ultrafast discrimination of Gram-positive bacteria and highly efficient photodynamic antibacterial therapy using near-infrared photosensitizer with aggregation-induced emission characteristics. Biomaterials, 2020, 230: 119582
35 He X, Yang Y, Guo Y, *et al.* Phage-guided targeting, discriminative imaging, and synergistic killing of bacteria by AIE bioconjugates. J Am Chem Soc, 2020, 142: 3959–3969
36 Li J, Wang J, Li H, *et al.* Supramolecular materials based on AIE luminogens (AIEgens): Construction and applications. Chem Soc Rev, 2020, 49: 1144–1172
37 Zhang Y, Zhao X, Li Y, *et al.* A fluorescent photosensitizer with far red/near-infrared aggregation-induced emission for imaging and photodynamic killing of bacteria. Dyes Pigments, 2019, 165: 53–57
38 Chen X, Huang L, Jia Y, *et al.* AIE-based theranostic probe for sequential imaging and killing of bacteria and cancer cells. Adv Opt Mater, 2020, 8: 1902191
39 Chen H, Li S, Wu M, *et al.* Membrane-anchoring photosensitizer with aggregation-induced emission characteristics for combating multidrug-resistant bacteria. Angew Chem Int Ed, 2020, 59: 632–636
40 Merchat M, Bertolini G, Giacomini P, *et al.* Meso-substituted cationic porphyrins as efficient photosensitizers of Gram-positive and Gram-negative bacteria. J Photochem Photobiol B-Biol, 1996, 32: 153–157
41 Zhang Y, Zheng K, Chen Z, *et al.* Rapid killing of bacteria by a new type of photosensitizer. Appl Microbiol Biotechnol, 2017, 101: 4691–4700
42 Brown ED, Wright GD. Antibacterial drug discovery in the resistance era. Nature, 2016, 529: 336–343
43 Perros M. A sustainable model for antibiotics. Science, 2015, 347: 1062–1064
44 Feng G, Yuan Y, Fang H, *et al.* A light-up probe with aggregation-induced emission characteristics (AIE) for selective imaging, naked-eye detection and photodynamic killing of Gram-positive bacteria. Chem Commun, 2015, 51: 12490–12493
45 Kang M, Zhou C, Wu S, *et al.* Evaluation of structure–function relationships of aggregation-induced emission luminogens for simultaneous dual applications of specific discrimination and efficient photodynamic killing of Gram-positive bacteria. J Am Chem Soc, 2019, 141: 16781–16789
46 Bennett LE, Ghiggino KP, Henderson RW. Singlet oxygen formation in monomeric and aggregated porphyrin c. J Photochem Photobiol B-Biol, 1989, 3: 81–89
47 Yan D, Wu Q, Wang D, *et al.* Innovative synthetic procedures for luminogens showing aggregation-induced emission. Angew Chem Int Ed, 2021, doi: 10.1002/anie.202006191
48 Liu GJ, Tian SN, Li CY, *et al.* Aggregation-induced-emission materials with different electric charges as an artificial tongue: Design, construction, and assembly with various pathogenic bacteria for effective bacterial imaging and discrimination. ACS Appl Mater Interfaces, 2017, 9: 28331–28338
49 Li Y, Hu X, Tian S, *et al.* Polyion complex micellar nanoparticles for integrated fluorometric detection and bacteria inhibition in aqueous media. Biomaterials, 2014, 35: 1618–1626
50 Li Q, Wu Y, Lu H, *et al.* Construction of supramolecular nanoassembly for responsive bacterial elimination and effective bacterial detection. ACS Appl Mater Interfaces, 2017, 9: 10180–10189
51 Ward JS, Nobuyasu RS, Batsanov AS, *et al.* The interplay of

thermally activated delayed fluorescence (TADF) and room temperature organic phosphorescence in sterically-constrained donor-acceptor charge-transfer molecules. Chem Commun, 2016, 52: 2612–2615
52 Grabowski ZR, Rotkiewicz K, Rettig W. Structural changes accompanying intramolecular electron transfer: Focus on twisted intramolecular charge-transfer states and structures. Chem Rev, 2003, 103: 3899–4032
53 Aoki S, Kagata D, Shiro M, *et al.* Metal chelation-controlled twisted intramolecular charge transfer and its application to fluorescent sensing of metal ions and anions. J Am Chem Soc, 2004, 126: 13377–13390
54 Zhang Q, Kuwabara H, Potscavage Jr. WJ, *et al.* Anthraquinone-based intramolecular charge-transfer compounds: Computational molecular design, thermally activated delayed fluorescence, and highly efficient red electroluminescence. J Am Chem Soc, 2014, 136: 18070–18081
55 DeRosa M. Photosensitized singlet oxygen and its applications. Coord Chem Rev, 2002, 233-234: 351–371
56 Devasagayam TPA, Kamat JP. Biological significance of singlet oxygen. Indian J Exp Biol, 2002, 40: 680–692
57 Lan M, Zhao S, Liu W, *et al.* Photosensitizers for photodynamic therapy. Adv Healthcare Mater, 2019, 8: 1900132
58 George S, Hamblin MR, Kishen A. Uptake pathways of anionic and cationic photosensitizers into bacteria. Photochem Photobiol Sci, 2009, 8: 788–795
59 Minnock A, Vernon DI, Schofield J, *et al.* Mechanism of uptake of a cationic water-soluble pyridinium zinc phthalocyanine across the outer membrane of *Escherichia coli*. Antimicrob Agents Chemother, 2000, 44: 522–527
60 Yuan H, Liu Z, Liu L, *et al.* Cationic conjugated polymers for discrimination of microbial pathogens. Adv Mater, 2014, 26: 4333–4338
61 Bai H, Yuan H, Nie C, *et al.* A supramolecular antibiotic switch for antibacterial regulation. Angew Chem Int Ed, 2015, 54: 13208–13213

Acknowledgements This work was supported by the National Natural Science Foundation of China (81572944 and 81971983), the CAS/SAFEA International Partnership Program for Creative Research Teams, the High-Level Entrepreneurship and Innovation Talents Projects in Fujian Province (2018-8-1), and the FJIRSM&IUE Joint Research Fund (RHZX-2018-004).

Author contributions Wang H, Pan X and Chen Z conceived and designed the project; Pan X designed the AIE PSs; Wang H and Wang Y synthesized the AIE PSs; Wang H performed the experiments; Wang H and Pan X analyzed the data; Liu W, Dai T and Yuan B provided the technical support; Pan X, Chen Z, Wang H and Chen X finished the writing.

Conflict of interest The authors declare that they have no conflict of interest.

Supplementary information Supporting data are available in the online version of the paper.

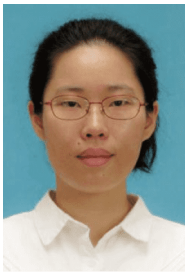

Huanhuan Wang received her BSc degree in chemistry from Shanxi University in 2017. She is currently a postgraduate under the supervision of Prof. Zhuo Chen at Fujian Institute of Research on the Structure of Matter (FJIRSM), Chinese Academy of Sciences (CAS). Her current research focuses on the design and synthesis of aggregation-induced emission photosensitizers and their antibacterial applications.

Xiaohong Pan received his PhD degree from the University of Pittsburgh in 2011 and his BSc degree from the University of Science and Technology of China in 2002. From 2011 to 2018, he worked at the Scripps Research in Florida as a research associate. He is currently an associate professor at FJIRSM, CAS. His research interest focuses on the design and synthesis of new photosensitizers for photodynamic therapy.

Zhuo Chen received her PhD degree from FJIRSM, CAS, following her MD degree from Fujian Medical University and her BSc degree from Chinese Pharmaceutical University. From 2001 to 2008, she worked on molecular pharmacology & therapeutics in Loyola University Chicago as a research associate. Her research focuses on tumor detection and targeted photodynamic therapy, including design and synthesis of new anticancer drug entities and evaluation of their pharmacological effects through experiments in cells and animals.

基于硝基苯甲酸结构的新型AIE光敏剂的光动力抗菌作用

王欢欢[1,2], 潘小宏[1*], 王亚琪[1], 刘雯珍[1], 戴涛[1,2], 袁彬彬[1], 陈学元[1,2], 陈卓[1,2*]

摘要 光动力疗法在抗菌领域中的应用备受关注. 传统的光敏剂在水性介质中容易聚集, 从而减少活性氧的产生并严重影响其光动力抗菌疗效. 为了减少传统光敏剂的聚集, 研究人员做出了许多努力. 与之相反, 聚集诱导发光型的光敏剂(AIE-PSs)利用其聚集的优势, 不仅增加了活性氧产量, 而且增强了荧光强度. 然而目前有关抗菌型AIE-PSs的研究仍处在发展阶段, 相关报道也非常有限. 我们在此首次报道了系列基于硝基苯甲酸结构的高效抗菌型AIE-PSs. 其中带负电荷的**TTVBA**不仅可选择性地灭杀球形细菌(如金黄色葡萄球菌), 而且易于被扩展成多种带正电荷且具有广谱抗菌性能的AIE-PSs(如**TTVBP1–3**). 我们发现, **TTVBP2**在125 nmol L^{-1}的低浓度下, 即可灭杀3.0 $\log_{10}$金黄色葡萄球菌; **TTVBP3**在1 μmol L^{-1}浓度下可灭杀4.7 $\log_{10}$表皮葡萄球菌, 在5 μmol L^{-1}浓度下可灭杀3.8 $\log_{10}$大肠杆菌, 成为目前已报道的最有效的抗菌AIE-PSs. 此外, 这些AIE-PSs直接与细菌混合后, 即对细菌具有出色的免洗成像能力. 因此, 我们认为基于硝基苯甲酸结构的**TTVBA**为未来高效抗菌光敏剂的设计提供了崭新思路.

